

Effect of Plasma Boundary and Electrode Asymmetry in Planar DC Discharges

A Thesis Submitted

In Partial Fulfillment of the Requirements

for the degree of

Doctor of Philosophy

by

Prashant Kumar Barnwal

to the



Department of Energy Science and Engineering
Indian Institute of Technology Delhi
New Delhi – 110016, India
June 2022

© Indian Institute of Technology Delhi (IITD), New Delhi, 2022

Dedicated to

... My Loving Family...

CERTIFICATE

This is to certify that the thesis entitled, “**Effect of Plasma Boundary and Electrode Asymmetry in Planar DC Discharges**”, submitted by **Mr. Prashant Kumar Barnwal**, to the Indian Institute of Technology, Delhi for the award of the degree of **Doctor of Philosophy**, is a bonafide record of the research work done by him under our supervision. The contents of this thesis, in full or in parts, have not been submitted to any other Institute or University for the award of any degree or diploma.

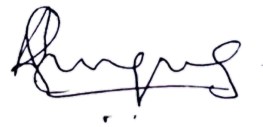


Prof. R. Narayanan

Dept. Energy Science and Engineering

IIT Delhi, New Delhi – 110016

India



Prof. A. Ganguli

Dept. Energy Science and Engineering

IIT Delhi, New Delhi – 110016

India

ACKNOWLEDGEMENTS

I take this opportunity to thank all the individuals who have directly or indirectly helped me to complete my thesis work.

I would like to express my sincere thanks and gratitude to my Ph. D. supervisors **Prof. Ramesh Narayanan** and **Prof. Ashish Ganguli** for their guidance and valuable advice during the tenure of this work. Foremost, I am deeply indebted to Prof. Ganguli, for his continuous support and encouragement at various stages of experiments, without which it may not be possible for me to complete this work. I humbly recognize his help in painstakingly correcting this thesis. I extend my deep regards to Prof. Narayanan for his consistent help in experiments and his kindness and constant motivation throughout my Ph.D. life. I, particularly acknowledge him for his insightful guidance during the learning of Langmuir Probe data analysis techniques.

I gratefully acknowledge **Prof. R. D. Tarey** for providing me with the necessary technical suggestions in experimental setup and diagnostic developments during my research pursuit. I would like to thank **Prof. Satyananda Kar**, for valuable discussions about the experimental plan at the initial stages of this work. I am also thankful to **Prof. Debaprasad Sahu**, and **Prof. Bibhuti Bhusan Sahu** for their suggestions and encouragement during the work.

I am highly obliged to thank **Mr. A. J. Josekutty** for his valuable and constructive suggestions during the planning and development of experimental work. His willingness to give his time so generously to all students has been very much appreciated. Thanks are also due to the technical staff of Plasma Lab **Mr. Hasmukh Kabariya**, and **Mr. Sumit Louhan**. Special thanks to Mr. Kabariya for his support during the development of the electrical circuit and the LABVIEW program for the data acquisition system.

I would like to thank my senior **Dr. Rahul Kumar** for the support and encouragement, I received from him. I sincerely acknowledge my colleagues and friends, **Arti Rawat, Anshu Verma, Priti Singh, Shweta Sharma, Mahreen,** and **Aishik Basu Mallick** for their help and support while working in the lab. It was a very nice experience to work with you all. Also, I am very grateful to **Dr. G. Veda Prakash**, Post Doc Fellow in Plasma Lab, IIT Delhi for sharing his research experience, his care and support are like an elder brother to me.

I extend my sincere thanks to **Mr. Sunil Bhogal** of Bhogal Precision Limited and **Mr. Birender Sharma** of the Glass Blowing Lab at IIT Delhi for the fabrication work undertaken by them. I am very much thankful to the MHRD, India for the Ph.D. scholarship.

I would like to express my deep sense of gratitude to my family who has been a vital pillar of support throughout this arduous journey. I would like to give special thanks to my Parents **Shri Ram Narayan Barnwal** and **Smt. Shrimawati Devi**, for being with me at every stage of my life and having endurance during my research work. Your prayer for me was what sustained me thus far. I am also thankful to my elder brother **Mr. Amit Barnwal** and younger brother **Vikrant** for their continuous support and love. I express my gratitude to my sister **Mrs. Vandana Barnwal** and my brother-in-law **Mr. Shailendra Barnwal** for their everlasting affection for me. And finally my dear nephews **Aarush** and **Ayansh**, their cute and innocent smiles always make me fresh and cool. This dissertation stands as a testament to your unconditional love, support, and patience.

Last but certainly not least, I would like to pay my regards to my spiritual friends for their strong associations and moral supports. I am eternally grateful to **H.G. Sarojmukha Madhav Prabhu ji** for the teachings of the underlying principles of life which helped me to keep motivated even in very tough situations. Finally, I bow down to the **Almighty Lord “Shri Krishna”** whose grace guided me from the very inception to the completion of this research work. Each moment during this work, I experienced the Grace of God, who continuously

enhanced my intelligence even at the moments of despair, inspired me to move forward, opened before me unexpected avenues, and enlightened my thoughts with His wisdom.



Prashant Kumar Barnwal

ABSTRACT

The work presented in this thesis focuses on the characterization of parallel plate DC discharges with various plasma confining boundaries. In DC discharges, it is standard practice to use a conducting vacuum vessel that is electrically grounded. Since the cathode is also grounded, the conducting chamber works as an extension of the cathode, providing an unlimited auxiliary cathode area relative to the anode. Such a system with a conducting chamber is labelled the Conducting Boundary or CB configuration in this work. To provide alternate boundary conditions to such a scenario, two more boundaries were considered. In one of these, the entire chamber wall along with other conducting surfaces were insulated with mica/glass tubes, *etc.* except the plasma-facing surfaces of electrodes. Such a system was termed the Large Volume Insulating Boundary (LVIB) configuration. One sees immediately that the latter configuration limits the cathode area severely. In effect, plasma in the entire chamber is driven by the planar anode and cathode only. To provide an alternative to the LVIB system in terms of volume, another insulated boundary system, the Small Volume Insulating Boundary (SVIB) system was configured, in which the electrodes are enclosed in a glass tube with mica sheets used for blocking from the top and bottom. It was observed that the discharge shows completely distinct behaviour with these two different boundaries (conducting and insulating). A relatively much higher discharge voltage is required to maintain the discharge in LVIB/SVIB than CB configuration. In addition to these, a leaky boundary was also created by introducing an annular gap in SVIB, which provides a new configuration termed the Leaky Boundary (LB) system in this work. LB discharges have exhibited several interesting nonlinear properties like Negative Differential Resistance (NDR), and hysteresis in their $V - I$ characteristics, anode glows that exhibit features like splitting into multiple blobs, spontaneous rotation of blobs, *etc.* Physically

and electrically, LB discharges are found either to operate in the SVIB mode or the CB mode, depending on the ratio of the Debye length (at the gap) to the gap width. If this ratio is greater than unity, the plasma produced in the glass tube is unable to escape into the outer conducting chamber and the LB discharge behaves predominantly as an SVIB discharge with almost matching $V - I$ characteristics. On the other hand, as the plasma density rises with increasing discharge current, a point is reached when the ratio of the Debye length to the gap width falls below unity and the plasma escapes into the outer conducting chamber. In the latter case, the $V - I$ characteristics of the LB discharge mimics that of the CB discharge. It is during the switch from the SVIB to CB regime of operation that the NDR mentioned above is observed.

A considerable portion of the investigations in this work pertains to anode glows. It is well known that the glow arises on account of electrons present in the anode sheath exciting the gas atoms as they are accelerated towards the anode. Now, the standard anode sheath is an electron-ion (e-i) sheath comprised of an ion layer (at the sheath edge) followed by a layer of electrons adjacent to the anode. (The presence of the ion layer depresses the potential within the sheath that helps push excess electrons back into the plasma.) However, in the present work, it was found the standard e-i sheath may be replaced by a pure ion sheath. Such types of sheaths are found in SVIB discharges, where electrons arriving at the anode in large numbers need to be heavily restricted (to match the discharge current). It turns out that it is possible to reverse this situation by *reducing the size of the anode drastically in comparison to that of the cathode* (labelled highly asymmetric case), so that *electron collection by the anode becomes highly inefficient* and the anode sheath has to revert back to the standard e-i sheath where anode glows are possible. It is possible to operate highly asymmetric LB discharges over a large range of discharge currents so that anode sheath is an e-i sheath that supports anode glows that exhibit various interesting features like splitting into twin or multiple blobs, fluctuations in their size, and intensities, rotations, *etc.* It is possible that the splitting into multiple anode blobs is

indicative of the existence of constricted current channels while the periodic rotation of the blobs within a specific current regime could be associated with a current-driven instability.

To summarize, the work undertaken in this thesis provides a systematic study of all the different discharge configurations (CB, LVIB, SVIB, and the LB) to determine their characteristic features and identify the various discharge regimes of operation that help the build-up to further interesting studies on anode sheaths / glows, mode switches, *etc.* Some of these features have been investigated in considerable detail.

शोध सार

इस थीसिस में प्रस्तुत कार्य विभिन्न प्लाज्मा सीमित सीमाओं के साथ समानांतर प्लेट डीसी डिस्चार्ज के लक्षण वर्णन पर केंद्रित है। डीसी डिस्चार्ज में, विद्युत रूप से ग्राउंडेड एक कंडक्टिंग वैक्यूम पोत का उपयोग करना मानक अभ्यास है। चूंकि कैथोड भी ग्राउंडेड है, इसलिए कंडक्टिंग चैंबर कैथोड के विस्तार के रूप में काम करता है, जो एनोड के सापेक्ष असीमित सहायक कैथोड क्षेत्र प्रदान करता है। एक संवाहक कक्ष के साथ इस तरह की प्रणाली को इस काम में कंडक्टिंग बाउंड्री या सीबी कॉन्फिगरेशन के रूप में लेबल किया जाता है। ऐसे परिदृश्य में वैकल्पिक सीमा की स्थिति प्रदान करने के लिए, दो और सीमाओं पर विचार किया गया। इनमें से एक में, इलेक्ट्रोड की प्लाज्मा-फेसिंग सतहों को छोड़कर, अन्य संवाहक सतहों के साथ पूरे कक्ष की दीवार को अभ्रक/ग्लास ट्यूबों आदि से अछूता किया गया था। ऐसी प्रणाली को लार्ज वॉल्यूम इंसुलेटिंग बाउंड्री (एलवीआईबी) कॉन्फिगरेशन कहा जाता है। एक तुरंत देखता है कि बाद वाला विन्यास कैथोड क्षेत्र को गंभीर रूप से सीमित करता है। वास्तव में, पूरे कक्ष में प्लाज्मा केवल प्लेनर एनोड और कैथोड द्वारा संचालित होता है। आयतन के संदर्भ में एलवीआईबी प्रणाली का विकल्प प्रदान करने के लिए, एक अन्य अछूता सीमा प्रणाली, स्मॉल वॉल्यूम इंसुलेटिंग बाउंड्री (एसवीआईबी) प्रणाली को कॉन्फिगर किया गया था, जिसमें इलेक्ट्रोड एक ग्लास ट्यूब में संलग्न होते हैं जिसमें ऊपर और नीचे से अवरुद्ध करने के लिए उपयोग की जाने वाली अभ्रक शीट होती है। यह देखा गया कि डिस्चार्ज इन दो अलग-अलग सीमाओं (संचालन और इन्सुलेट) के साथ पूरी तरह से अलग व्यवहार दिखाता है। सीबी कॉन्फिगरेशन की तुलना में एलवीआईबी / एसवीआईबी में डिस्चार्ज को बनाए रखने के लिए अपेक्षाकृत बहुत अधिक डिस्चार्ज वोल्टेज की आवश्यकता होती है। इनके अलावा, एसवीआईबी में एक कुंडलाकार अंतराल को शुरू करके एक लीकी सीमा भी बनाई गई थी, जो इस

काम में लीकी बाउंड्री (एलबी) सिस्टम नामक एक नया कॉन्फ़िगरेशन प्रदान करती है। एलबी डिस्चार्ज ने कई दिलचस्प नॉनलीनियर गुणों का प्रदर्शन किया है जैसे कि नेगेटिव डिफरेंशियल रेजिस्टेंस (एनडीआर), और उनके वी-आई विशेषताओं में हिस्टैरिसिस, एनोड ग्लो जो कई बूँदों में विभाजित होने, ब्लॉक्स के सहज रोटेशन आदि जैसी विशेषताओं को प्रदर्शित करता है। शारीरिक और विद्युत रूप से, एलबी डिस्चार्ज या तो एसवीआईबी मोड या सीबी मोड में संचालित होता है, जो डिबाई लंबाई (गैप पर) और गैप की चौड़ाई के अनुपात पर निर्भर करता है। यदि यह अनुपात एक से अधिक है, तो ग्लास ट्यूब में उत्पादित प्लाज्मा बाहरी संचालन कक्ष में बाहर निकलने में असमर्थ है और एलबी डिस्चार्ज मुख्य रूप से लगभग मिलान वी-आई विशेषताओं के साथ एसवीआईबी डिस्चार्ज के रूप में व्यवहार करता है। दूसरी ओर, जैसे-जैसे प्लाज्मा घनत्व, बढ़ते डिस्चार्ज करंट के साथ बढ़ता है, एक बिंदु पर पहुँच जाता है जब डिबाई लंबाई और गैप की चौड़ाई का अनुपात एक से नीचे हो जाता है और प्लाज्मा बाहरी संवाहक कक्ष में निकल जाता है। बाद के मामले में, एलबी डिस्चार्ज की वी-आई विशेषताएँ सीबी डिस्चार्ज की नकल करती हैं। यह एसवीआईबी से सीबी के संचालन के शासन में स्विच के दौरान है कि ऊपर उल्लिखित एनडीआर देखा जाता है।

इस काम में जांच का एक बड़ा हिस्सा एनोड ग्लो से संबंधित है। यह सर्वविदित है कि एनोड शीथ में मौजूद इलेक्ट्रॉनों के कारण ग्लो उत्पन्न होती है क्योंकि वे गैस परमाणुओं को उत्तेजित करते हैं और एनोड की ओर त्वरित होते हैं। अब, मानक एनोड शीथ एक इलेक्ट्रॉन-आयन (ई-आई) शीथ है जिसमें आयन परत (शीथ किनारे पर) शामिल होता है, जिसके बाद एनोड से सटे इलेक्ट्रॉनों की एक परत होती है। (आयन परत की उपस्थिति शीथ के भीतर क्षमता को कम करती है जो अतिरिक्त इलेक्ट्रॉनों को प्लाज्मा में वापस धकेलने में मदद करती है।) हालांकि, वर्तमान कार्य में, यह पाया गया कि मानक ई-आई शीथ को शुद्ध आयन शीथ द्वारा प्रतिस्थापित किया जा सकता है। एसवीआईबी डिस्चार्ज में इस तरह के शीथ पाए जाते हैं, जहां बड़ी संख्या में एनोड पर पहुंचने वाले इलेक्ट्रॉनों को (डिस्चार्ज करंट से मेल खाने के लिए) भारी प्रतिबंधित करने की आवश्यकता होती है। यह पता चला है कि कैथोड (अत्यधिक

असममित मामले के रूप में लेबल) की तुलना में एनोड के आकार को काफी कम करके इस स्थिति को उलटना संभव है, ताकि एनोड द्वारा इलेक्ट्रॉन संग्रह अत्यधिक अक्षम हो जाए और एनोड शीथ को वापस करना पड़े वापस मानक ई-आई शीथ पर जहां एनोड ग्लो संभव है। डिस्चार्ज धाराओं की एक बड़ी रेंज पर अत्यधिक असममित एलबी डिस्चार्ज को संचालित करना संभव है ताकि एनोड शीथ एक ई-आई शीथ है जो एनोड ग्लो का समर्थन करता है जो विभिन्न दिलचस्प विशेषताओं को प्रदर्शित करता है जैसे कि जुड़वां या कई बूँदों में विभाजित, उनके आकार में उतार-चढ़ाव, और तीव्रता, घुमाव, आदि। यह संभव है कि कई एनोड ब्लॉक्स में विभाजन संकुचित वर्तमान चैनलों के अस्तित्व का संकेत है, जबकि एक विशिष्ट वर्तमान शासन के भीतर ब्लॉक्स के आवधिक रोटेशन को वर्तमान-संचालित अस्थिरता से जोड़ा जा सकता है।

संक्षेप में, इस थीसिस में किए गए कार्य उनकी विशिष्ट विशेषताओं को निर्धारित करने के लिए सभी अलग-अलग डिस्चार्ज कॉन्फिगरेशन (सीबी, एलवीआईबी, एसवीआईबी, और एलबी) का एक व्यवस्थित अध्ययन प्रदान करते हैं और ऑपरेशन के विभिन्न डिस्चार्ज शासनों की पहचान करते हैं जो एनोड शीथ / ग्लो, मोड स्विच आदि पर और दिलचस्प अध्ययन के बिल्ड-अप में मदद करते हैं। इनमें से कुछ विशेषताओं की काफी विस्तार से जांच की गई है।

CONTENTS

Certificate.....	(i)
Acknowledgments.....	(iii)
Abstract.....	(vii)
List of Figures.....	(xix)
List of Tables.....	(xxv)
1. Introduction.....	1
1.1 DC Discharge plasma.....	3
1.1.1 Fundamental concepts.....	4
1.1.2 Literature survey.....	9
1.2 Motivation.....	15
1.3 Outline of work in the thesis.....	17
1.4 Objectives of thesis.....	19
1.5 Plan of the thesis.....	20
2. Experimental setup and diagnostic tools.....	23
2.1 Introduction.....	23
2.2 Experimental system.....	23
2.3 Experimental configurations.....	25
2.3.1 Conducting boundary (CB) configuration.....	25
2.3.2 Large volume insulating boundary (LVIB) configuration.....	26

2.3.3	Small volume insulating boundary (SVIB) configuration.....	26
2.3.4	Leaky boundary (LB) configuration.....	29
2.4	Measurements and diagnostics.....	30
2.4.1	Voltage – Current ($V_d - I_d$) characteristics of discharge.....	30
2.4.2	Langmuir probe.....	31
2.4.3	Photographs and video recordings.....	40
2.5	Operating regime of discharge.....	40
3.	Characterization of discharges in conducting boundary (CB) and insulating boundary (IB) configurations.....	41
3.1	Introduction.....	41
3.2	Discharge characterization.....	41
3.2.1	CB Configuration.....	41
3.2.2	LVIB Configuration.....	43
3.2.3	SVIB Configuration.....	43
3.3	Plasma characterization.....	45
3.3.1	CB Configuration.....	45
3.3.2	LVIB Configuration.....	50
3.3.3	SVIB Configuration.....	52
3.3.3.1	Other studies in SVIB configuration.....	53
3.3.3.2	Anode sheath drop in SVIB discharges.....	56
3.4	Comparative study of SVIB and LVIB configurations.....	58
3.5	Summary and conclusion.....	59
4.	Negative Differential Resistance (NDR) induced by leaks in insulated boundary discharge.....	61
4.1	Introduction.....	61

4.2 Discharge characteristics with leaking boundary.....	62
4.2.1 Discharge characteristics for different gaps and pressures.....	62
4.2.2 Temporal behaviour.....	66
4.2.3 Variation with pressure and anode size.....	67
4.2.4 ‘Kink’ in LBD characteristics.....	71
4.3 Plasma characterization.....	74
4.4 Comparative analysis of the different configurations.....	76
4.5 Summary and conclusion.....	79
5. Anode glows in highly asymmetric electrode discharges – observation of rotating anode glows.....	81
5.1 Introduction.....	81
5.2 Characterization of LBDs with highly asymmetric electrodes.....	83
5.3 Anode glows with highly asymmetric electrodes (≈ 8 mm anode).....	84
5.3.1 Glows at low pressure (≈ 600 mTorr).....	84
5.3.2 Anode glows at moderate pressures (≈ 1200 mTorr).....	87
5.4 Rotating anode glows at high pressure.....	90
5.5 Summary and conclusion.....	97
6. Conclusions and future scope of work.....	99
6.1 Summary of thesis.....	99
6.2 Future scope of work.....	102
References.....	103
List of Publications.....	115
Author’s Biography.....	119

LIST OF FIGURES

Figure 1.1: A typical planar geometry DC Discharge setup.

Figure 1.2: (a) Voltage controlled NDR in which the current is single-valued (I) for multiple voltages (V_a , V_b , and V_c), it is also called N-Type NDR, (b) current controlled NDR in which voltage is single-valued (V) for multiple current (I_a , I_b , and I_c), also called S-type NDR. Red lines in both the plots represent the NDR region whereas the blue lines are the PDR regions.

Figure 1.3: (a) Configuration of coaxial electrodes (Coax A) with central anode and vacuum chamber being at ground potential and the coaxial outer electrode (cathode) being maintained at a negative potential [132] and (b) Configuration of coaxial electrodes (Coax B) with central anode being the powered electrode and the coaxial outer electrode (cathode) and vacuum chamber being at ground potential [133].

Figure 2.1: Schematic diagram of the vacuum chamber, LP: Langmuir probe.

Figure 2.2: Photograph of the experimental setup.

Figure 2.3: Schematic diagram of experimental system configurations. (a) CB configuration: discharge can come in contact with conducting ss chamber (b): LVIB configuration: Discharge is allowed to expand into a large volume with insulating boundary. Here “1”, “2”, and “3” represent anode, cathode, and probe tip respectively.

Figure 2.4: Schematic diagram of experimental system configurations; (a) SVIB configuration: Discharge is enclosed inside a small insulating Boundary, EFGH. (b) LB configuration: Discharge is allowed to escape from the small insulated

volume (EFGH) into the outer conducting volume (ABCD) via the annular gap between EF and E'F'. Here “1”, “2”, and “3” represent anode, cathode, and probe tip respectively.

Figure 2.5: Circuit diagram for recording discharge characteristics.

Figure 2.6: photograph of the langmuir probe with the scale (bottom) given for reference.

Figure 2.7: Schematic diagram of the Langmuir probe.

Figure 2.8: Circuit diagram for recording LP characteristics.

Figure 2.9: (a) Typical LP characteristics for CB configuration with symmetric electrodes, at 1000 mTorr pressure and 5 mA discharge current, and (b) Plot of the natural log of electron current versus probe bias voltage (V_B).

Figure 2.10: (a) Typical LP characteristics for SVIB configuration with symmetric electrodes, at 1000 mTorr pressure and 5 mA discharge current, and (b) Plot of the natural log of electron current versus probe bias voltage (V_B).

Figure 3.1: Comparison of discharge characteristics in CB and LVIB configuration for symmetric electrode system.

Figure 3.2: Discharge characteristics in SVIB configuration; (a) Variation with gas pressure, (b) Variation with anode size.

Figure 3.3: Axial variation of plasma parameters in CB configuration for different sizes of anode at $p = 1000$ mTorr and $I_d = 5$ mA.

Figure 3.4: LP analysis plot for (a) CB-symmetric case, showing single electron temperature, (b) CB-asymmetric case, two linear slopes in $\ln(I_e)$ versus V_B plot represent the presence of two electron populations.

Figure 3.5: Axial variation of different plasma parameters in LVIB configuration.

Figure 3.6: Axial variation of plasma parameters in SVIB configuration with different anode sizes at $p = 1000$ mTorr and $I_d = 5$ mA.

Figure 3.7: Plasma parameters at different pressures in SVIB configuration.

Figure 3.8: (a) LP characteristics at different I_d in SVIB configuration, (b) Variation of different plasma parameters with increasing I_d in SVIB configuration.

Figure 3.9: Schematic diagram to show nature of anode sheath (a, b) and Variation of sheath voltage, V_s inside the anode sheath (c, d). (a) ion-rich sheath, (b) electron-rich sheath; (c) Electron rich sheath with $\Delta V < 0$ showing alternate layers of positive and negative charges. (d) Pure ion sheath with only positive charges within the sheath for $\Delta V > 0$.

Figure 3.10: (a) Comparison of discharge characteristics in LVIB and SVIB for different pressures, (b) comparison of plasma parameters in LVIB and SVIB for a wide range of pressure.

Figure 4.1: (a) Leaky boundary (LB) configuration: Plasma can escape from gap in the SVIB system (EFGH) into the outer CB system (ABCD) through the annular gap (EF - E'F'). (b) Discharge characteristics of LB system for different gap widths showing sudden jump from SVIB to CB behaviour.

Figure 4.2: Comparison of discharge characteristics in SVIB, CB, and LB ($g \approx 5$ mm) configurations for a wide range of pressures (800-1200 mTorr).

Figure 4.3: (a) Simultaneous plot of supply voltage [V_{sup}], discharge current [I_d] and discharge voltage [V_d] with respect to time, (b) Discharge characteristics along with hysteresis in LB configuration at $p = 1200$ mTorr with 38 mm anode diameter.

Figure 4.4: $V_d - I_d$ characteristics in LB (≈ 5 mm gap) configuration at $p = 1200$ mTorr showing the NDR on the forward path between c – d and an NDR on the return path between j – k: (a) 38 mm electrode; (b) 8 mm electrode.

Figure 4.5: $V_d - I_d$ characteristics in LB configuration for: (a) different pressures ≈ 800 to 1400 mTorr with ≈ 38 mm anode; (b) four different sizes of anode at $p = 1200$ mTorr.

Figure 4.6: Variation of V_p , V_a and ΔV with I_d for (a) symmetric electrode system [$\varphi_a = \varphi_c = 76$ mm], and (b) highly asymmetric electrode system [$\varphi_a = 8$ mm, and $\varphi_c = 76$ mm] at $p = 1200$ mTorr.

Figure 4.7: (a) Variation of V_p , V_a and ΔV with I_d for anode size, = 76 mm; (b) Axial variation of V_p with respect to V_a , at different I_d . (i) $I_d = 1.5$ mA, (ii) $I_d = 2.5$ mA, and (iii) $I_d = 5$ mA.

Figure 4.8: Plasma snapshot (a) before ($I_d = 8$ mA) and (b) after the NDR ($I_d = 17$ mA) for 38 mm anode diameter at 1200 mTorr Pressure, and 5 mm annular gap. Here, white strips represent the plasma facing surface edge of electrodes (anode and cathode).

Figure 4.9: Plasma parameter variation with I_d in LB discharges for ≈ 38 mm anode, gap $g \approx 5$ mm at $p \approx 1200$ mTorr.

Figure 5.1: (a) Schematic diagram of Leaky boundary (LB) configuration with highly asymmetric electrodes. Plasma can escape from the leak in the SVIB system (EFGH) into the outer CB system (ABCD) through the annular gap between EF and E'F'; here '1', '2' and '3' represent the anode, cathode, and probe tip respectively and AG denotes anode glow (see also figure 2.4 of chapter 2); (b) $V_d - I_d$ characteristics of LB discharges with highly asymmetric electrodes over a large pressure range.

Figure 5.2: $V_d - I_d$ characteristics in SVIB, CB, and LB (gap ≈ 5 mm) discharges at ≈ 600 mTorr pressure.

Figure 5.3: Images of anode glows at $p \approx 600$ mTorr in SVIB discharges for, (a) $I_d \approx 0.8$ mA, (b) $I_d \approx 1.2$ mA, (c) $I_d \approx 1.8$ mA, and (d) $I_d \approx 2.2$ mA; in CB discharges for, (a') $I_d \approx 2$ mA, (b') $I_d \approx 15$ mA, (c') $I_d \approx 30$ mA, and (d') $I_d \approx 45$ mA, and in LB discharges (gap ≈ 5 mm) for, (a'') $I_d \approx 1$ mA, (b'') $I_d \approx 1.75$ mA, (c'') $I_d \approx 12$ mA, and (d'') $I_d \approx$

20 mA. Here the white strip ‘AS’ and ‘CS’ in (a) indicates the location of anode surface and cathode surface respectively.

Figure 5.4: $V_d - I_d$ characteristics at $p \approx 1200$ mTorr in LB configuration with ≈ 8 mm anode and ≈ 5 mm gap.

Figure 5.5: Plasma parameter variation with increasing I_d in highly asymmetric LB discharges for ≈ 8 mm anode, gap, $g \approx 5$ mm at $p \approx 1200$ mTorr.

Figure 5.6: Evolution of anode glow with increasing discharge current (I_d) in LB configuration across the NDR at $p = 1200$ mTorr. Here the white strip ‘AS’ and ‘CS’ in (a) indicates the location of anode surface and cathode surface respectively. Before NDR: (a) $I_d \approx 0.5$ mA, (b) $I_d \approx 1.0$ mA, (c) $I_d \approx 2.0$ mA, (d) $I_d \approx 2.5$ mA, (e) $I_d \approx 3.0$ mA, (f) $I_d \approx 5.0$ mA, (g) $I_d \approx 7.0$ mA, (h) $I_d \approx 10.0$ mA, and after the NDR: (i) $I_d \approx 22.0$ mA, (j) $I_d \approx 30.0$ mA, (k) $I_d \approx 35.0$ mA, (l) $I_d \approx 40.0$ mA. Remaining LB specifications are same as in figure 5.5.

Figure 5.7: (a) LB discharge characteristics at 2000 mTorr pressure with highly asymmetric electrode in LB configuration; (b) Variation of plasma parameters with I_d in for the LB discharges in (a).

Figure 5.8: Images of anode glows in LBDs at $p \approx 2000$ mTorr for different current (a) $I_d \approx 5$ mA, (b) $I_d \approx 7$ mA, (c) $I_d \approx 10$ mA, (d) $I_d \approx 18$ mA, and (e) $I_d \approx 24$ mA before NDR; (f) $I_d \approx 43$ mA after the NDR. Remaining LB specifications are same as in figure 5.7 (a).

Figure 5.9: Time synchronized images of anode glows captured by Front and Right cams to illustrate rotation of the two blobs. Synchronization was achieved by a laser flash recorded by both cameras (seen as a red / orange blob) in the image “e”. The images at “e”, “g”. and “i” correspond to a more complete set of images (taken by the Front

cam) shown in figure 5.10. The LBDs were initiated at $p \approx 2000$ mTorr and $I_d \approx 7$ mA with remaining specifications same as in figure 5.7 (a).

Figure 5.10: Temporal variation of anode glow intensity (captured by Front cam) at $p \approx 2000$ mTorr and $I_d \approx 7$ mA. The sequence of images from ‘a’ to ‘i’ represents a half period of rotation. (a) $t \approx 0$, (b) $t \approx 0.2$ s, (c) $t \approx 0.4$ s, (d) $t \approx 0.6$ s, (e) $t \approx 0.8$ s, (f) $t \approx 1.0$ s, (g) $t \approx 1.2$ s, (h) $t \approx 1.4$ s, (i) $t \approx 1.6$ s. The blobs have maximum separation at (a) $t \approx 0$, after a quarter cycle rotation the blobs are seen to merge at (e) $t \approx 0.8$ s, and after another quarter cycle rotation, the balls are separated again after “swapping” at (i) $t \approx 1.6$ s. Remaining LB specifications are same as in figure 5.7 (a).

Figure 5.11: Variation of light intensity (arbitrary units) from the blobs (captured by the Front cam) derived from MatLab’s Image Processing Toolbox. Each intensity peak corresponds to the center of a blob, and the spatial intensity variation about the peak gives the variation of light intensity within the blob. The horizontal axis gives radial distance (in pixels) from the anode center, with 100 pixels ≈ 8 mm. The blobs have maximum separation (≈ 14 mm) at $t \approx 0$ and nearly zero separation at $t \approx 0.8$ s. At $t \approx 1.6$ s, the blobs are separated once again, with the blobs interchanged. The LB discharges were initiated at $p \approx 2000$ mTorr and $I_d \approx 7$ mA. Remaining LB specifications are same as in figure 5.7 (a).

Figure 5.12: Pixel calibration: The anode (dia ≈ 8 mm) is used to calibrate the pixels. It is found that 100 pixels ≈ 8 mm. At maximum separation, the two blobs have a separation of $d \approx 14$ mm. The diameter of blob “1” ≈ 8.5 mm and that of blob “2” ≈ 7.4 mm. The LB discharges were initiated at $p \approx 2000$ mTorr and $I_d \approx 7$ mA. Remaining LBD specs are same as in figure 5.7 (a).

LIST OF TABLES

Table 3.1: Ionization efficiencies for the different populations for different anode sizes (For CB configuration, at $p = 1000$ mTorr, $I_d = 5$ mA, and $z =$ average over the discharge length).

Table 4.1: λ_{De} values ≈ 6 mm in front of the anode ($\varphi_a \approx 38$ mm) for data taken from figure 4.5 (a).

Table 4.2: Comparison of plasma parameters for CB, SVIB and LB discharges ($p = 1200$ mTorr, $I_d = 5$ mA) with anode diameter = 38 mm and cathode diameter = 76 mm.